Deep oxidative desulfurization with simultaneous oxidative denitrogenation of diesel fuel and straight run gas oil

Jorge F. Palomeque-Santiago[a],[*], Ricardo López-Medina[b], Raúl Oviedo-Roa[a], Juan Navarrete-Bolaños[a], Rodolfo Mora-Vallejo[a], J. Ascención Montoya-de la Fuente[a], José Manuel Martínez-Magadán[a]

[a] Instituto Mexicano del Petróleo, Av. Eje Central Lázaro Cárdenas Norte 152, Col. San Bartolo Atepehuacan, 07730 Ciudad de México, México
[b] Universidad Autónoma Metropolitana Unidad Azcapotzalco, Av. San Pablo N° 180, Col. Reynosa Tamaulipas, 02200 Ciudad de México, México

ARTICLE INFO

ABSTRACT

High levels of sulfur organic compounds (SOCs) and nitrogen organic compounds (NOCs), which are contaminants present in diesel fuel and straight run gas oil (SRGO), were removed using tungsten/zirconia catalysts and hydrogen peroxide by oxidative desulfurization and oxidative denitrogenation reactions. Two tungsten sources were used: tungstic acid and ammonium metatungstate. The catalysts obtained by anionic exchange at low pH with tungstic acid showed remarkable homogeneity and high W dispersion attributed to tetrahedral W species and full dibenzothiophene (DBT) oxidation was achieved in 5 min of reaction. On the other hand, the catalysts obtained by impregnation with ammonium metatungstate developed mainly octahedral species with less DBT oxidation. It was also found that tetrahedral species generate more acidity than octahedral species. A density functional theory computational study confirmed the observed DBT oxidation trend shown by tetrahedral and octahedral W species on the peroxide-activated catalysts. Diesel fuel and SRGO were desulfurized and denitrogenated to a high extent: 97% in diesel fuel and 70% in SRGO for sulfur compounds and 96% in diesel fuel and 89% in SRGO for nitrogen compounds, whereas C_1–C_3 dibenzothiophenes, 4-methyl dibenzothiophene, and 4,6-dimethyl dibenzothiophene were fully removed. The elimination of SOCs and NOCs present in fuels can be effectively carried out in a single process to obtain clean fuels.

1. Introduction

Diesel fuel is one of the most important fuels used for transportation. EPA's Clean Air Highway Diesel fuel final rule requires a sulfur content in highway diesel fuel of 15 ppm, creating immediate health benefits, and allowing engine manufacturers to begin using advanced emission control systems that will further reduce harmful emissions. Hydrodesulfurization is a costly process and many difficulties arise out of producing ultra-low sulfur diesel fuel (ULSD), because it requires the application of severe operating conditions and the use of special active catalysts [1]. Oxidative desulfurization (ODS) has very good prospects to help obtain ULSD, but up to date, any commercial unit has been built. For the successful industrial implementation of the ODS processes, substantial achievements are required to develop highly active and selective catalysts for the oxidation of sulfur compounds and process designs for effective desulfurization technology [2]; the use of tungsten/zirconia catalysts in ODS seems to be a promising option.

An efficient heterogeneous process is a topic of interest due to the possibility of reusing solid catalysts. Several systems using solid catalysts have been investigated to oxidize sulfur compounds; the reaction times of most of the reported systems are long; it is then desirable to develop solid catalysts which perform the oxidation reactions in short reaction times, which is important for industrial applications. WO_x/ZrO_2 catalysts have demonstrated to be a good option in these reactions, because they create strong acid sites [3–5] and reach high conversions of sulfur compounds [6–8]; these catalysts are usually prepared by wet impregnation with ammonium metatungstate solutions. We have reported that tungsten/zirconia catalysts prepared from tungstic acid and hydrogen peroxide reach 100% of DBT conversion in the first 5 min of reaction; this high activity has been attributed to tetrahedral W species that remain isolated even at high concentrations [9,10].

Another important topic in the elimination of environmental pollutants from fuels is the removal of nitrogen compounds. It has attracted the attention of both the industry and the researchers' community, because they have been identified as strong inhibitors of

hydrodesulfurization reactions for diesel fuel production [11,12]. Other methods used to obtain clean fuels by eliminating nitrogen compounds have been reported [13–17]. Simultaneous desulfurization and denitrogenation processes have already been studied by adsorption [18–20], ionic liquids [21,22] and simultaneous oxidative desulfurization and denitrogenation [23–25]. The extensive research carried out in the denitrogenation of hydrocarbons gives an idea of the importance of this process.

The impregnation method with ammonium metatungstate has been widely used for many years for preparing WO_x/ZrO_2 catalysts. The main characteristic found in this system is its high acidity with activity for different reactions [26–28]. The use of the H_2WO_4–H_2O_2 acid solution is not a common method used to prepare WO_x/ZrO_2 catalysts by anion exchange, and there are many features that are still unknown; the high activity found in DBT oxidation in an oxidative desulfurization reaction was reported in a previous study [9]. In this work, these catalysts were extrapolated to the oxidative desulfurization and oxidative denitrogenation of diesel fuel and SRGO, achieving a high degree of removal of these contaminants. The differences regarding two sources of tungsten species (tungstic acid and ammonium metatungstate) are studied as functions of the spatial arrangement, acidity and dispersion of W species. The effects of the spatial arrangement are theoretically studied through density functional theory.

2. Experimental and theoretical methodology

2.1. Catalysts

Commercial zirconium hydroxide from Mel Chemicals with surface area of $400 \, m^2/g$ was used. The anion exchange was performed using 2 g of powder and 50 mL of a 0.2 M solution prepared from tungstic acid (H_2WO_4, 99%) in hydrogen peroxide (H_2O_2, aq. 30%). The process was performed in an Erlenmeyer flask for 4 h at room temperature with continuous stirring (TA). Another sample was prepared by impregnation with 50 mL of a 0.2 M aqueous solution of ammonium metatungstate ($(NH_4)_6[H_2W_{12}O_{40}] \, nH_2O$, 99%) at its natural pH (AM). The suspensions were filtered, washed with deionized water and dried in an oven at 100 °C. Theses samples were calcined in air flow at 700 °C for 4 h (TA-700 and AM-700, respectively).

2.2. Characterizations

Tungsten content was determined by plasma emission spectrophotometry in a Perkin-Elmer 5000 spectrometer. BET surface areas were obtained under vacuum by nitrogen physisorption in an ASAP-2405 analyzer from Micromeritics. Powder x-ray diffraction patterns were obtained in a D-500 SIEMENS diffractometer with CuKα1 radiation. Ultraviolet–visible (UV–vis) spectra were obtained in a dual-beam Varian Cary 1 spectrophotometer, in diffuse reflectance mode, employing an integration sphere accessory. Raman spectra were recorded at room temperature with a Dilor XY spectrometer with triple monochromator. The exciting line at 514.53 nm of an Ar-Kr laser was focused, using a long-distance 50× objective. The used output power was 5 mW with a spectral resolution of 3.09. The Fourier transform infrared (FTIR) technique by pyridine adsorption was used to determine the type of acid sites. Experiments were carried out in a Nicolet FTIR spectrometer 170-SX model. Prior to pyridine adsorption, the samples were outgassed and then heated up to 500 °C at 20 °C/min and cooled down to room temperature. After this pre-treatment, they were exposed to saturated pyridine vapor for 20 min. After adsorption, infrared spectra were recorded after outgassing at 25, 100, 200, 300 and 400 °C. Scanning electron microscopy analysis was performed by using a JEOL 440 scanning electron microscope operated at an accelerating voltage of 25 kV and 20.000× magnification. A sample was covered with Au-Pd and made ready for analysis by fixing it to the device sample holder with the help of a carbon sticky band. Another analysis was performed

in a Zeiss SUPRA 55VP equipment operated at an accelerating voltage of 2 kV and 1.000× magnification.

2.3. Catalytic tests

2.3.1. ODS reaction

The experiments were carried out at 60 °C as an optimal-previously-reported temperature [29]. γ-Butyrolactone (98%) was chosen as a good solvent for the sulfones produced in the ODS reactions [30]. In a typical experiment, a solution composed by 9200 ppm (w/v) of dibenzothiophene (98%) in 10 mL of solvent and 100 mg of catalyst were placed in a three-neck, 50-mL-round-bottom micro-reactor equipped with a magnetic stirrer; 0.51 mL of hydrogen peroxide (H_2O_2, aq. 30%) were added and considered as the starting reaction time. Samples were taken at time intervals and the reaction products were analyzed by GC-Mass in an HP6890 series II plus chromatograph equipped with an HP-5MS 60 m, 0.25 mm and 25 μm column and a 5973 mass selective detector operating in the chemical ionization mode. A calibration curve was made with a correlation coefficient of 0.9933. The dependence of the DBT conversion versus time was obtained for all the experiments.

2.3.2. Diesel fuel and SRGO reaction

Hydrotreated diesel fuel (338 ppm of total sulfur) and SRGO (16,370 ppm of total sulfur) were also subjected to the ODS reaction; 20 mL of solvent (γ-butyrolactone, 98% or methanol, 99.9%), 20 mL of hydrocarbon and 200 mg of catalyst were placed in a 50-mL reactor with vigorous magnetic stirring. Hydrogen peroxide was added at a H_2O_2/sulfur molar ratio of 20. Samples were taken at time intervals and the catalyst was separated by filtration. The sulfur compounds in diesel fuel were determined by gas chromatography in a Varian 3600, equipped with a sulfur chemiluminescence detector and a crosslinked methyl silicon column, 50 m × 0.32 mm. Total sulfur and total nitrogen were determined in an Antek 9000 analyzer by UV fluorescence and chemiluminescence, respectively.

2.4. Quantum mechanical modeling

Density functional theory (DFT), as implemented in the DMol³ module of the BIOVIA Materials Studio (BMS) software, was used to calculate the reaction energies of the DBT oxidation by tetrahedral and octahedral single tungsten oxide clusters in order to investigate theoretically which tungsten oxygen coordination leads to a better performance.

The energy of all molecular models was calculated through spin unrestricted runs of the BMS DMol³ geometry optimization task by using the Generalized Gradient corrected functional by Perdew and Wang (GGA/PW91), the Ortmann–Bechstedt–Schmidt method for DFT dispersion correction, the Double Numerical plus Polarization (DNP) basis set, the DFT Semi-core Pseudopotentials for core treatment, a smearing value of 0.005 Ha for orbital occupancy, and coarse option settings for all remaining parameters.

Each reaction energy ΔE was determined by the difference $E_P - E_R$ among the energy E_P of a product, and the energy E_R of the reactants.

3. Results and discussion

3.1. Characterization of the catalysts

3.1.1. Textural properties

Table 1 shows the characteristics of the exchanged and supported solids treated at different temperatures. It is well known that the anion exchange of terminal OH^- anions by bigger WO_4^{2-} anions prevents Zr sintering, maintaining high surface areas. The tungsten surface densities of dried solids are very far from the saturation of the monolayer surface coverage of WO_x on ZrO_2 (4.5 or 7.3 W/nm^2), and far from the surface density at which maximum catalytic activity is obtained for *o-*

Table 1

Textural properties of the dried solids after impregnation or ion exchange, and of the solids calcined at 700 °C.

	Dried at 100 °C		Calcined at 700 °C	
	AM	TA	AM-700	TA-700
Surface area (m^2/g)	226	270	85	96
Tungsten content (wt %)	18.0	24.2	16.2	22.5
Tungsten surface density (W/nm^2)	2.6	2.9	6.2	7.7

xylene isomerization (10 W/nm^2) or DBT oxidation (6–8 W/nm^2) [6,26,31]; however, after calcination at 700 °C, the tungsten surface densities reached the mentioned saturation monolayer.

3.1.2. X-ray diffraction patterns

As expected, both dried samples were amorphous, showing either high dispersion of the oxide phase on the zirconia support surface or the presence of WO$_x$ nanocrystals. After treatment at 700 °C, the tetragonal phase was stabilized in both samples. In AM-700, the WO$_3$ phase was detected (2θ = 23.1, 23.6 and 24.4); on the other hand, the WO$_3$ phase was not found in TA-700 (patterns not shown).

3.1.3. UV–vis spectroscopy

The UV–vis diffuse reflectance is a technique used to characterize the electronic structure of solids. In this region of the electromagnetic spectrum, electronic intra-molecular transitions take place as a consequence of light absorption. In these phenomena, electrons are transferred from a ligand orbital of the metal orbitals or vice versa, generating absorption charge transfer spectra (Ligand Metal Charge Transfer, LMCT, or Metal-Ligand Charge Transfer, MLCT). Charge transfer processes frequently lie at the blue end of the visible region or in the ultraviolet region [32]. The impregnated AM-700 solid presents an absorption band near 210 nm, associated with zirconia in a tetragonal phase, and a pronounced shoulder near 250 nm (Fig. 1). On the other hand, the TA-700 exchanged catalyst shows a broad plateau between 200 and 300 nm. These kinds of spectra have been observed on 12-phosphotungstic acid/TiO$_2$ [18] and W-MCM systems, which were associated with high dispersion of the WO$_x$ species [33].

3.1.4. Raman spectroscopy

Raman spectroscopy is a powerful technique in the study of supported tungsten catalysts, providing surface and bulk phase information
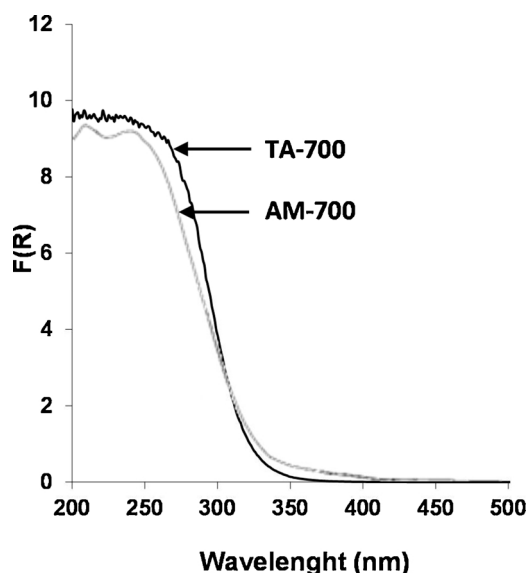

Fig. 1. UV–vis spectra of calcined catalysts at 700 °C.

and the W interaction with supports. The Raman spectra (Fig. 2) show great differences according to the preparation method. The AM catalyst (prepared with ammonium metatungstate and dried at 100 °C) shows signals at 960 cm^{-1} and a broad band near 840 cm^{-1}. These bands have been associated with monotungstate compounds, made up of WO$_4$ tetrahedral W−O symmetric stretching, and with W−O−W stretching modes, respectively [5,34,35]; they have also been assigned to symmetric and asymmetric stretching modes, respectively, of WO$_4^{2-}$ tetrahedral molecular ions [36]. The calcined sample presents the characteristic intense and sharp bands of WO$_3$ with high crystallinity at 715 and 810 cm^{-1} corresponding to W=O bending and W=O stretching modes, respectively [37].

The dried TA catalyst presents the same WO$_x$ species as AM, but the band at 840 cm^{-1} is more pronounced, which is indicative of stronger interactions with the support. When treated at 700 °C, a broadening band appears at around 900 cm^{-1}, assigned to the W−O−Zr stretching vibration mode which characterizes the bond anchoring WO$_x$ species to the support [3,35]. The signals at 820 and 1015 cm^{-1} are attributed to the W−O−W stretching vibration mode and to the symmetric stretch of the terminal W=O of monotungstates, which indicates that polytungtates coexist with monotungstates [38]; there is no evidence of crystalline WO$_3$, which is in agreement with the DRX analysis. It is noteworthy that the TA-700 sample shows a signal at 640 cm^{-1}, which is assigned to the ZrO$_2$ tetragonal phase.

It has been reported that W/Zr solids with low W content develop tetrahedral species, while with values above 13%, the W species take an octahedral symmetry [39]. The TA-700 catalyst, synthesized by anion exchange and having a W concentration of 22.5%, behaved very differently, maintaining tetrahedral species; the width of the bands may indicate a broad distribution of geometrically different species having variable W−O bond orders [35].

3.1.5. Scanning electron microscopy

The micrographs of calcined and impregnated catalysts (AM-700) show materials, where the tungsten species are well dispersed on the surface, forming clusters with large particles; on the contrary, in the calcined and exchanged catalysts (TA-700), higher homogeneity is perceived with smaller particle sizes and without the formation of large clusters (Fig. 3).

3.1.6. Pyridine adsorption-FTIR spectroscopy

It is well known that some species such as sulfates and phosphates enhance acidity when they are supported on zirconia, giving place to the formation of very stable Brønsted and Lewis acid sites. In a special way, the presence of Brønsted sites is related to an intimate relationship between cations (SO$_4^{2-}$, PO$_4^{3-}$ and WO$_4^{2-}$) and ZrO$_2$, forming a kind of solid solution at the surface [40]. Pyridine adsorption on solids, followed by FTIR, is the most popular technique to measure and characterize the types of acid sites. Fig. 4a shows the pyridine adsorption spectra of the AM-700 sample, where a band characteristic of the pyridinium ion formed on Brønsted acid sites is observed at 1540 cm^{-1}; on the other hand, the absorption peak at 1447 cm^{-1} is attributed to pyridine coordinately bonded to Lewis acid sites.

Spectra of the TA-700 catalyst (Fig. 4b) show very intense bands at 1640 (PyH$^+$), 1540 (PyH$^+$) and 1490 cm^{-1} (ν19a) that are present even at 400 °C (Brønsted acid sites). Besides these bands, there are other intense bands at 1613 (ν8a, ν8b), 1490 (ν19a) and 1450 cm^{-1} (ν19b), which are related to the presence of Lewis acid sites [41]. The broad band centered at 1450 cm^{-1} shows a shoulder at 1440 cm^{-1}, mainly at low temperatures, which disappears revealing the true Lewis sites when the temperature is above 100 °C; these pyridine molecules may be attributed to physically adsorbed pyridine, interacting with OH groups with low acidity [42]. This behavior is completely different from to the first one; the signals of Brønsted and Lewis sites are clearly more intense and more defined and agree with the Raman spectroscopy results, where the sample structures with surface WO$_4^{2-}$ species generate
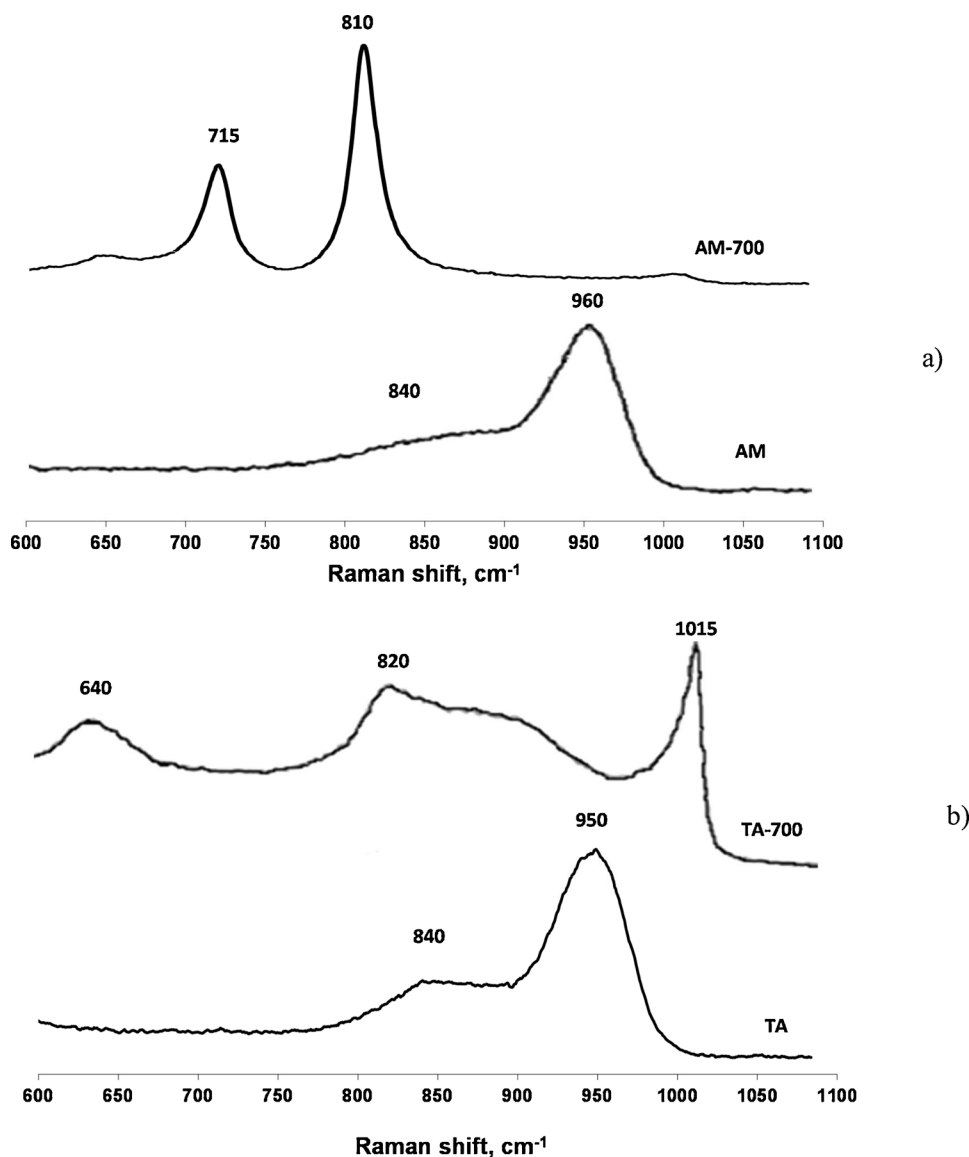
Fig. 2. Raman spectra: a) impregnated catalysts, and b) exchanged catalysts.

strong and stable acid sites (Brønsted and Lewis), while crystalline O_h species of WO_3 with a polymeric octahedral complex generate less acidity.

The number of Brønsted and Lewis sites (as mmol/g) were computed by integration of the bands with absorption maxima at 1540 and 1450 cm^{-1} from the pyridine adsorption-FTIR analysis at the different desorbed temperatures (Fig. 4); the results are summarized in Table 2. It can be appreciated that the anion exchange method creates one order of magnitude more acidity than the impregnation method. The bands at 1640 and 1613 cm^{-1}, associated with the strength of Brønsted and Lewis sites, respectively, are very intense, remaining at 400 °C, where a number of these strong acid sites are still present at this temperature. This fact means that the anion exchanged catalyst has weak and strong Brønsted and Lewis sites, reflecting the presence of different acid strengths. On the contrary, the impregnation catalyst has mostly weak acid sites that only remain up to 300 °C.

3.2. DBT oxidation

The catalysts were tested in the oxidation of dibenzothiophene. Sulfone was the only oxidation product obtained. Conversions on dried and exchanged catalysts were high as expected, demonstrating that

tetrahedral W species are very active for the ODS reaction, attaining total conversion in 3 min of reaction (Fig. 5a). AM reached a lower DBT conversion rate, which maybe was induced by the octahedral species. DBT conversion on the calcined TA-700 catalyst was at the same level of its dried precursor, but AM-700 enhanced its DBT conversion (Fig. 5b). As seen in Table 3, the catalysts prepared by anion exchange have 2.5 and 3.3 times more activity than those prepared by the impregnation method. These values are one order of magnitude higher with respect to other catalytic systems for ODS reactions [43,44]. The AM uncalcined catalyst seems to have higher initial rate than the calcined AM-700. Both catalysts have similar W loadings, but the former has higher surface area, where the active sites may be more exposed to react. Notwithstanding, when comparing the TOF of both catalysts, the calcined one has better activity.

The differences between the tungsten/zirconia catalysts prepared by anion exchange with peroxotungstic acid and the catalysts prepared from ammonium metatungstate can be well established from DRX, UV–vis, SEM and Raman spectroscopy; higher homogeneity can be perceived with the tungstic acid preparation. Other differences are important to be pointed out: the use of H_2O_2 in the TA preparation is the key to the high activity of this catalyst. The pH of the H_2WO_4–H_2O_2 solution was less than 1, this acidic solution is favorable for the
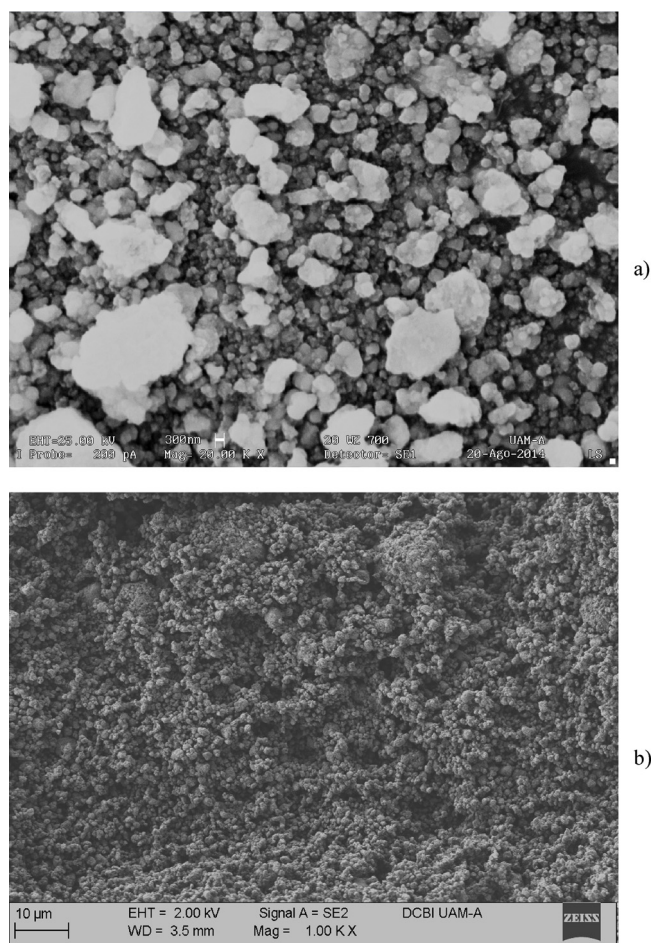
a)

b)

Fig. 3. Micrographs of: a) AM-700, and b) TA-700.

exchange of OH^- by WO_4^- anions. When using solutions with different W concentrations, different W loadings are obtained, while this loading is independent of the solution concentration when using ammonium metatungstate [9]. Another important difference is that the H_2WO_4–H_2O_2 acid solution mainly generates WO_4^- anions while in acid ammonium metatungstate solutions, aggregated species are formed [45,46].

Figueras et al. studied the H_2WO_4-H_2O_2/ZrO_2 system and by making several Raman analyses at different points of the same sample, they found high homogeneity, which was in contrast with those prepared using ammonium metatungstate [47]. The catalyst obtained by anion exchange generated tetrahedral species even at high W loading with lower tendency to form clusters than the solids prepared from ammonium metatungstate. The tetrahedral species are more strongly anchored to the support in a wide geometrical distribution, which may be responsible of the elevated Lewis and Brønsted acidity in comparison with the octahedral species obtained with the impregnation preparation method.

The relationship between the high DBT conversion in short reaction times and the characteristics of the exchanged catalyst can be discussed in the following terms: Since the TA catalysts have higher capacity of W loading, the surface coverage is remarkably enhanced, because of the high dispersion of tungsten species attested by the absence of WO_3 crystals; the origin of this high coverage is related to the strong interaction between the support and the promoter [48]. From the Raman analyses, the band at around 900 cm^{-1} in TA-700 is associated with W−O−Zr bonds, showing strong interactions between tungsten and the support; this band is absent in AM-700, which suggests weaker interactions between W and Zr. Valigi et al. concluded that tungsten forms

strong Zr−O−W bonds and also W−O−W bonds from small polymeric tungsten species directly anchored to the zirconia surface. The Raman broad WO_x band in the 900–1000 range cm^{-1} reflects the heterogeneity of the surface species [5].

The surface coverage of WO_x on ZrO_2 has been related to the number of acid sites [26,48]; the maximum concentration of acid sites has been calculated between 5–8 W/nm^2 which is related to the W monolayer coverage and the activity; at lower and higher tungsten loads, the acidity and catalytic activity were lowered. The TA-700 catalyst is close to those coverage values, showing high DBT oxidation levels, however, the dried TA catalyst is far below that surface coverage, but even so, its performance in the DBT oxidation is still high. These results suggest that the highest W dispersion and the presence of tetrahedral species, associated with their high acidity, notably improve the oxidative desulfurization reactions.

3.3. Structure

The spatial geometry of the WO_x species seems to play an important role. The tetrahedral phase formed on zirconia has been well established by different reports: Di Gregorio and Keller determined the chemical environment of tetrahedral W species by XPS analyses, revealing that WO_3/ZrO_2 contains W(V) and W(VI) surface species [49]. The increase in Brønsted acidity has been reported to be due to a configuration change from edge-shared to corner-shared as in the tetrahedral WO_4 groups [50]. Tetrahedral and octahedral species may also be present on the zirconia surface when WO_3/ZrO_2 catalysts are prepared with ammonium metatungstate [51,52], but when the tungsten load is higher than the monolayer surface coverage, the predominant species are in octahedral coordination. These differences in geometry make the acid sites grow differently in both tungsten phases. By the condensation phenomenon, tetrahedral isolated species can be present without forming large clusters, and the Brønsted and Lewis sites are generated through W(V) and W(VI), respectively [49]; on the other hand, octahedral species generate mainly Brønsted and Lewis sites through W(VI) [32,52].

Results by Galano et al. showed that Brønsted acidity plays an important role in oxidative desulfurization reactions, suggesting that the combined presence of Lewis and Brønsted sites facilitates the OOH addition process to the catalyst [6]; in our experimental results, such a combination was found in the catalyst prepared by anionic exchange with peroxotungstic acid.

3.4. Oxidation mechanism and quantum mechanical modeling

The oxidation mechanism of sulfur compounds is known to be carried out by a peroxometal pathway involving transition elements with d° configuration such as Mo(VI) and W(VI) without a final change in the metal oxidation state [53]. It is known that organic sulfur compounds are oxidized by hydrogen peroxide via a heterolytic process involving the nucleophilic attack of the sulfur atom on oxygen [54]. The reactivity of sulfur compounds in the sulfoxidation reaction is correlated to the nucleophilicity of the sulfur atom. When *tert*-Butyl hydroperoxide is used as oxidant in the presence of a molybdenum catalyst, the coordination of hydroperoxide to Mo−O is prompted by the polarization of the $Mo^{\delta+}$−$O^{\delta-}$ bond [55]. A similar hydroperoxytungstate intermediate has been proposed when using hydrogen peroxide and a Na_2WO_4/Al_2O_3 catalyst through W(VI) species [56].

Several mechanisms have been proposed for the oxidation of sulfur compounds via ODS [57–59]. According to García-Gutiérrez et al., active hydroperoxytungstate species can be formed by the nucleophilic attack of hydrogen peroxide on W(VI) catalyst atoms. The oxidation of the sulfur atom in the organosulfur compounds must proceed then by nucleophilic attack of an active hydroperoxytungstate to form sulfoxide and regenerated tungstate species; subsequently, the sulfoxide undergoes further oxidation by the hydroperoxytungstate species to form
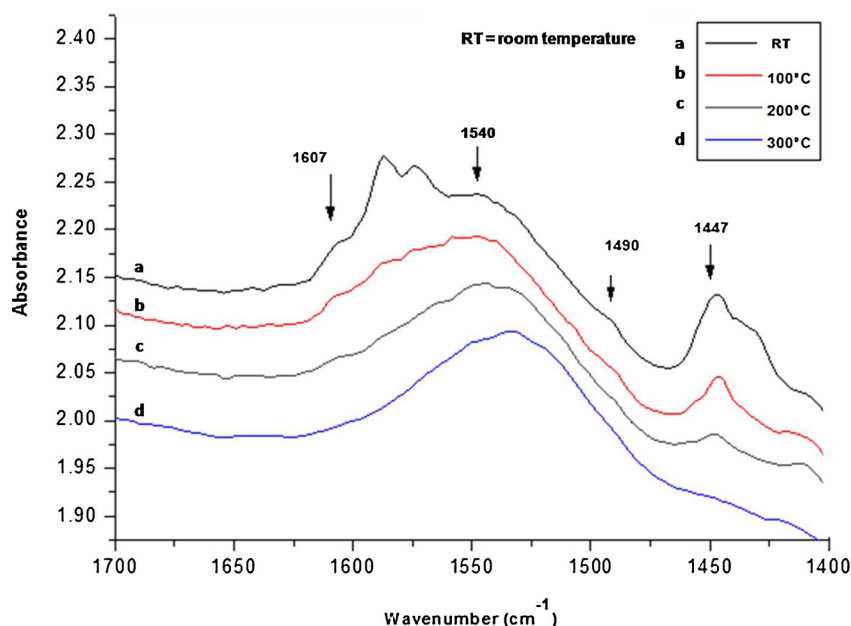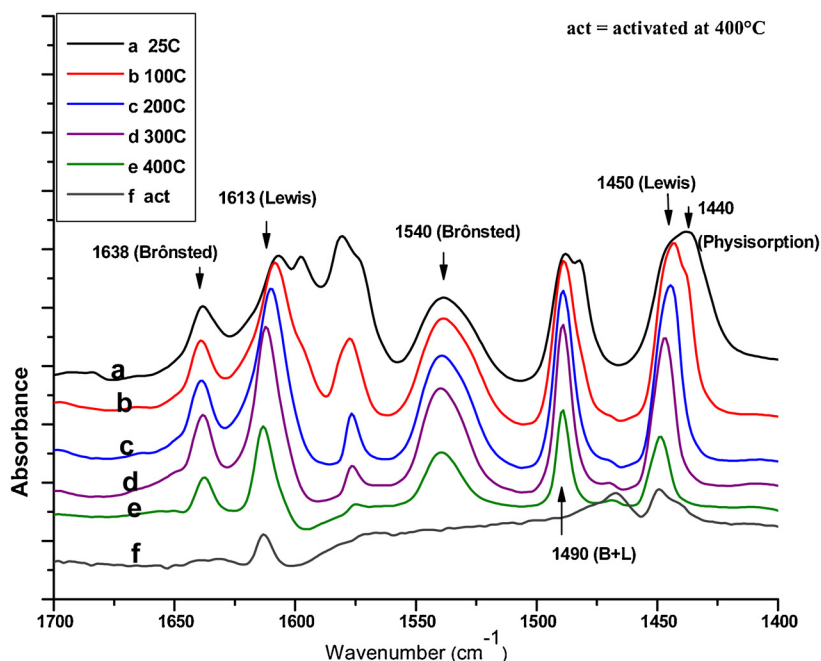
Fig. 4. Pyridine adsorption: a) AM-700, and b) TA-700.

sulfone. This oxidation mechanism was corroborated in the present work by DFT computations using molecular models of DBT and hydrogen peroxide interacting with electrically neutral tetrahedral WO_4H_2 and charged octahedral $[WO_6H_5]^{-1}$ clusters, which have two and one exposed oxygen atoms, respectively. It is worth mentioning that it is necessary the tungsten oxide clusters have, at least, one exposed oxygen to be able to form the hydroperoxytungstate species by breaking the O—O peroxide bond.

The reaction energies to form DBT sulfoxide and DBT sulfone are given in Figs. 6 and 7. The total of the reaction energies to obtain DBT sulfoxide, followed by its conversion to sulfone, gives -131.20 and -92.72 kcal/mol in tetrahedral and octahedral tungsten clusters, respectively; thus, the tetrahedral coordination releases more energy

(38.48 kcal/mol; 42%) than that of the octahedral coordination during the DBT oxidation.

It was found that the catalyst activation by H_2O_2 occurs on the Lewis acid sites since, during the activation reaction, one of the ·OH hydroxyl radicals from the broken peroxide forms a bond with the catalyst tungsten (Figs. 6a and 7a). Also from these figures, it was found that the catalyst activation occurs preferably at those sites having octahedral coordination since the formation of the hydroperoxytungstate is 2.3 times more exothermic than at tetrahedral ones. On the contrary, once the catalyst has been activated, the DBT oxidation occurs at the Brønsted acid sites, but not at the Lewis ones since DBT or its sulfoxide captures oxygen from the OH groups of the activated catalyst (Figs. 6b and 7b for DBT oxidation, and Figs. 6c and 7c for DBT sulfoxide

Table 2

Surface acidity of WO_x/ZrO_2 determined by pyridine-adsorbed FTIR (mmol/g catalyst).

Temperature (°C)	Impregnation method			Anion exchange method		
	Brønsted	Lewis	Total acidity	Brønsted	Lewis	Total acidity
50	0.033	0.070	0.103	0.229	0.477	0.706
100	0.018	0.023	0.041	0.266	0.325	0.591
200	0.006	0.020	0.026	0.233	0.226	0.459
300	0	0.015	0.015	0.163	0.139	0.302
400	0	0	0	0.070	0.074	0.144
Total	0.057	0.128	0.185	0.961	1.241	2.202
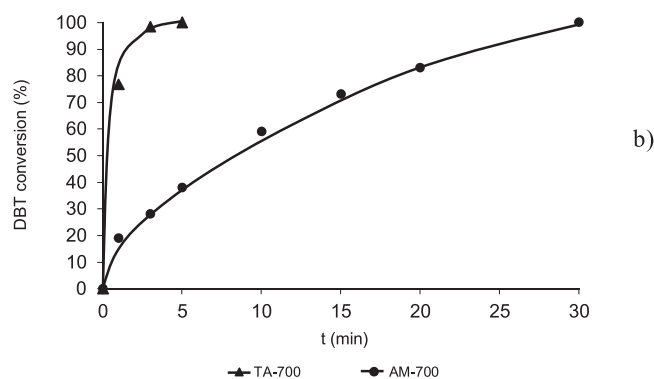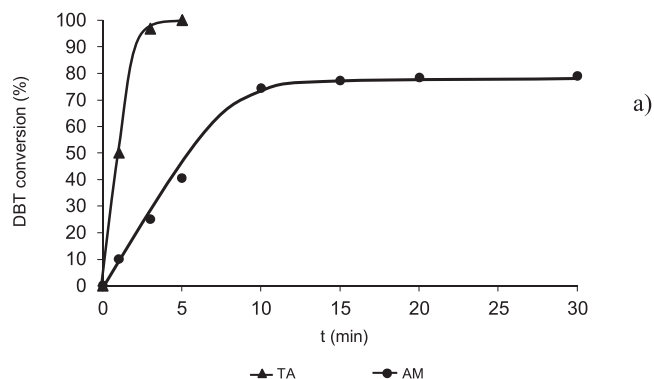
Fig. 5. DBT conversion of catalysts a) dried at 100 °C, and b) calcined at 700 °C.

Table 3

TOF calculated as mol of DBT or S reacted per total mol of W, in s^{-1}.

	TA	AM	TA-700	AM-700
DBT	2.79	0.85	4.49	1.80
Diesel fuel	–	–	2.06	–
SRGO	–	–	77.92	–

oxidation). These figures show that the DBT oxidation takes place preferably at those activated sites having tetrahedral coordination because DBT sulfoxide and DBT sulfone formations release factors of 1.57 and 1.33 times, respectively, which is more energy than at the octahedral ones, suggesting that the acid strength of the activated catalyst, as inferred by the ODS reactions, is modulated by the oxygen coordination around tungsten atoms.

The performance of the hydroperoxide based at the tetrahedral tungstate cluster can be understood in the framework of the molecular orbitals (Fig. 8). It is known that a reaction takes place by electron transfer from the Highest Occupied Molecular Orbital (HOMO) of a molecule to the Lowest Unoccupied Molecular Orbital (LUMO) of
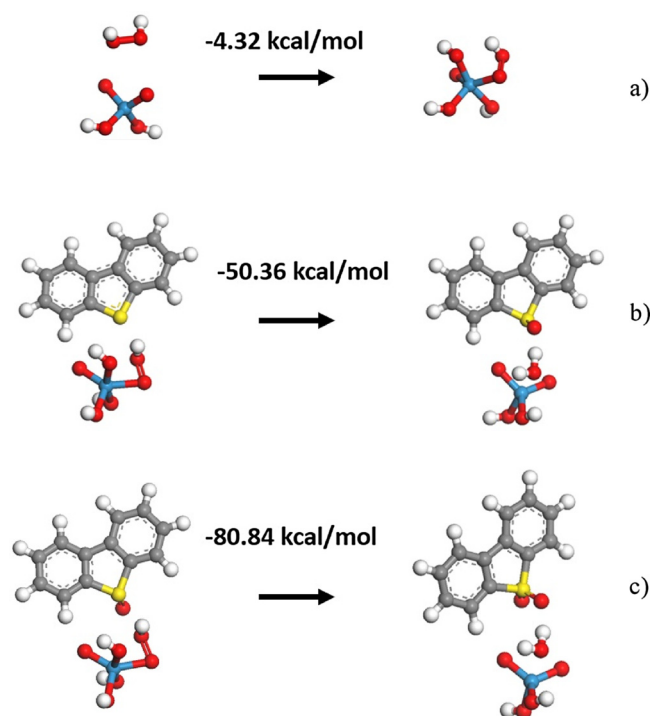
Fig. 6. a) Formation of the hydroperoxytungstate species at the tetrahedral WO_4H_2 cluster. b) Conversion of DBT to DBT sulfoxide. c) Conversion of DBT sulfoxide to DBT sulfone.
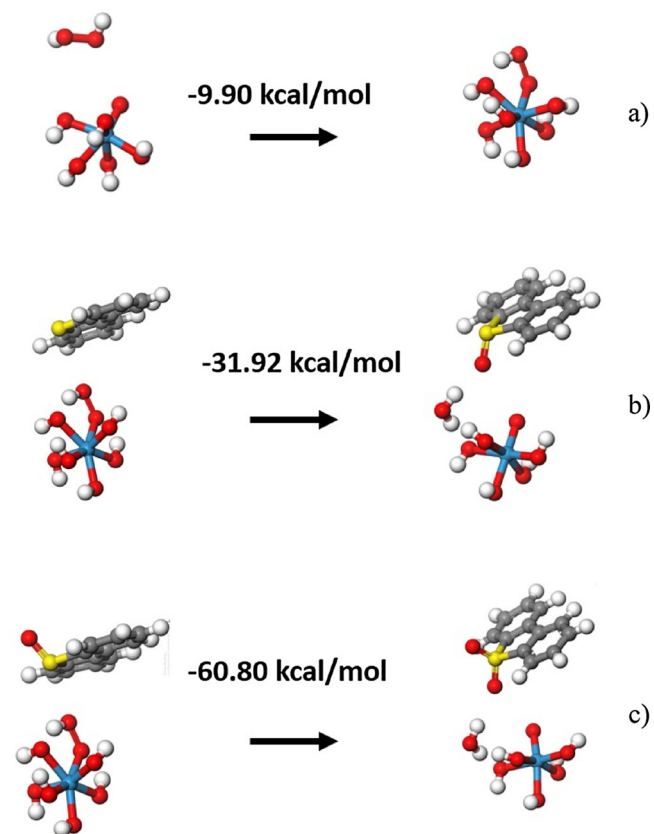
Fig. 7. a) Formation of the hydroperoxytungstate species at the octahedral $[WO_6H_5]^{1-}$ cluster. b) Conversion of DBT to DBT sulfoxide. c) Conversion of DBT sulfoxide to DBT sulfone.
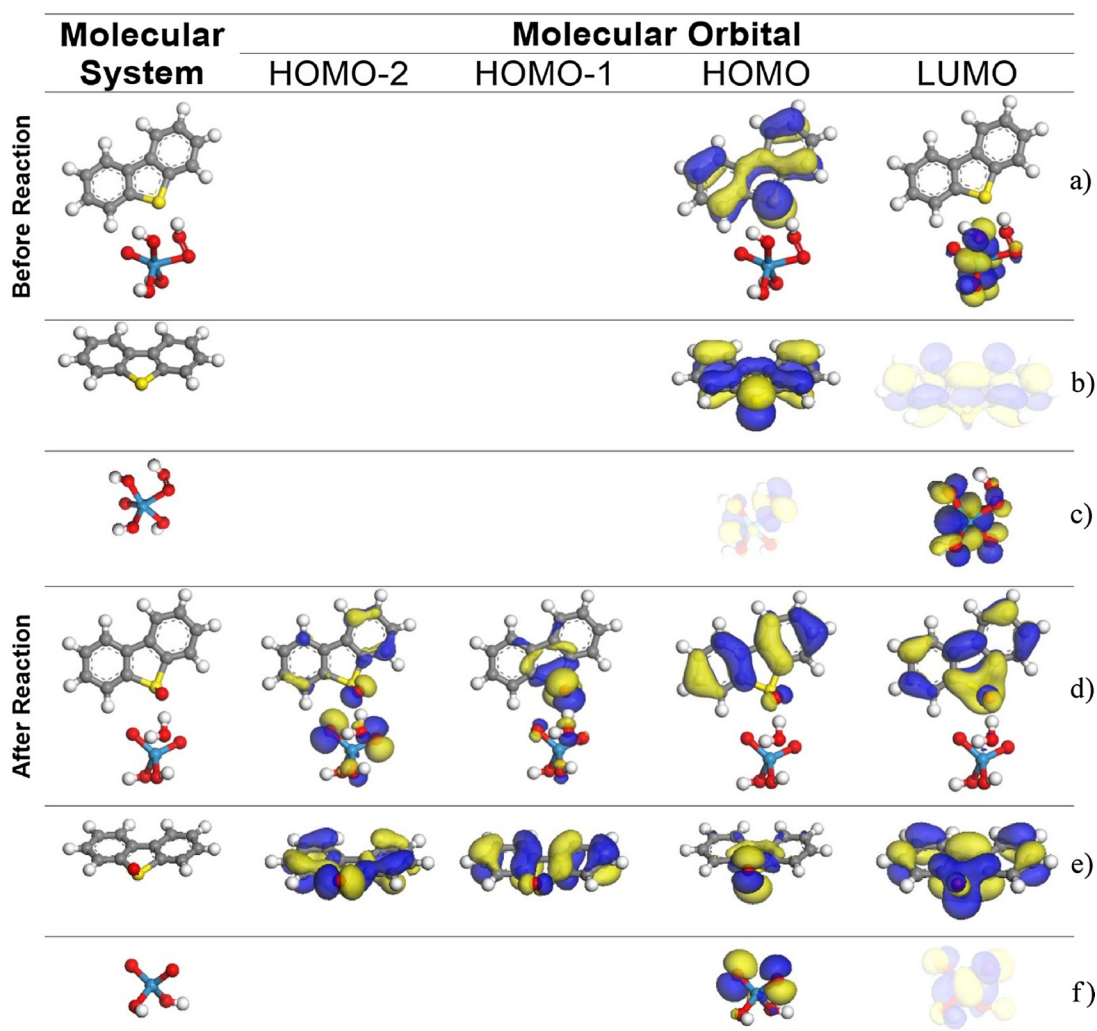
Fig. 8. Molecular mechanism for the conversion from DBT to DBT sulfoxide by a hydroperoxide formed at a tetrahedral tungstate. Molecular orbitals for: a) the system composed of a DBT prior to the reaction with the hydroperoxytungstate species WO_6H_4, b) a single DBT, c) a single hydroperoxytungstate species WO_6H_4, d) the system composed of the products DBT sulfoxide, water and tetrahedral tungstate WO_4H_2 obtained after reaction, e) single DBT sulfoxide, and f) single tetrahedral tungstate WO_4H_2. Decolored molecular orbitals for single molecules denote those molecular orbitals that are not shown in the reactant and product systems.

another one. When a single DBT molecule approaches the tetrahedral cluster (Fig. 8a), the reaction occurs by the DBT HOMO (Fig. 8b) and the catalyst LUMO (Fig. 8c). It is worth noting that the catalyst LUMO is antibonding, i.e., when it is occupied, the catalyst becomes unstable. After reaction, the activated catalyst is indeed decomposed and then the original tetrahedral tungstate is recovered (Fig. 8d), and, in fact, the LUMO of the system of products (DBT sulfoxide + water + WO_4H_2) is not extended over WO_4H_2, but only over DBT sulfoxide instead, i.e., this reaction deactivated the hydroperoxytunsgate.

A detailed analysis of the molecular orbitals of the products' system (Fig. 8d) reveals that the products' HOMO-2 is composed of the HOMO-2 of single DBT sulfoxide (Fig. 8e) and from the HOMO of the single WO_4H_2 (Fig. 8f). By definition, any state HOMO-n is energetically below HOMO, i.e., is hardly accessible to participate in reactions; then, WO_4H_2 is stabilized in front of the DBT sulfoxide. Moreover, HOMO and HOMO-1 of the single DBT sulfoxide (Fig. 8e) are interchanged in the products' system, which means that the HOMO of the products' system is less antibonding than the one of the single DBT sulfoxide, and therefore, DBT sulfoxide becomes also stable in front of WO_4H_2.

Conversely, before reaction in the octahedral system, the HOMO and LUMO of the reactants' system formed by DBT and the tungstate-based hydroperoxide catalyst (Fig. 9a) are constituted by the HOMO of the single catalyst (Fig. 9c) and the LUMO of DBT (Fig. 9b),

respectively. Consequently, the electrons must be transferred from the octahedral catalyst to DBT, i.e., in the opposite direction to that occurring at the tetrahedral system. This step exposes a stronger HOMO-1 bonding of the octahedral catalyst; therefore, the catalyst will have difficulty in ceding oxygen atoms. Effectively, after reaction (Fig. 9d), HOMO and LUMO of the products' system (DBT sulfoxide + water + octahedral tungstate) are just the HOMO-1 of single octahedral tungstate (Fig. 9f) and the LUMO of single DBT sulfoxide.

From the above described molecular mechanisms, it is inferred that the tetrahedral oxygen coordination around tungsten is favored over the octahedral because through the former, more energy is released by transferring electrons from DBT to recover the original catalyst, maintaining the catalyst continuously available whereas the octahedral oxygen coordination releases lower energy since electrons are transferred from the catalyst to DBT, reinforcing the catalyst bonding character, making more difficult the catalyst recovery.

3.5. Surface acidity

As mentioned above, the catalytic activity of WO_x/ZrO_2 systems has been strongly correlated to their acid sites and in turn, to the W surface coverage. Brønsted acid sites have been related to catalytic activity in the isomerization of alkanes [3], methanol dehydration [26] and
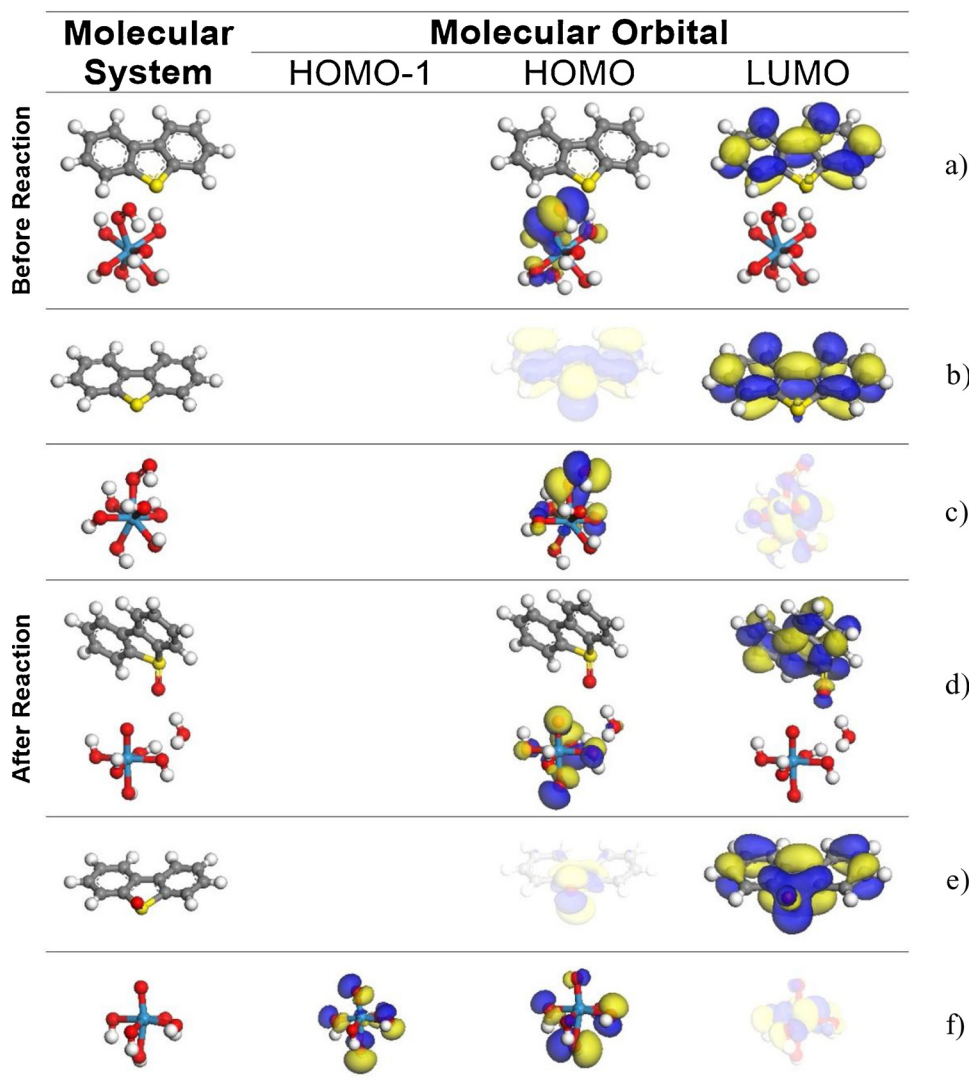
Fig. 9. Molecular mechanism for the conversion from DBT to DBT sulfoxide by a hydroperoxide formed at an octahedral tungstate. Molecular orbitals for a) the system composed of a DBT before the reaction with the hydroperoxytungstate species $[WO_8H_7]^{1-}$, b) a single DBT, c) a single hydroperoxytungstate species $[WO_8H_7]^{1-}$, d) the system composed of the products DBT sulfoxide, water and octahedral tungstate WO_4H_2 obtained after reaction, e) single DBT sulfoxide, and f) single tetrahedral tungstate $[WO_6H_5]^{1-}$. Decolored molecular orbitals for single molecules denote those molecular orbitals that are not shown in the reactant and product systems.

esterification of levulinic-acid esters [61], among others. The strength increase in Brønsted acidity has been considered the responsible for the enhancement of the catalytic activity, which is also increased as the tungsten loading up to a limit of the monolayer coverage. The tungsten active species seem to be different on both preparations; in the impregnation method, below the monolayer coverage, isolated monotungstate species predominate on the zirconia surface. These species are difficult to reduce and thus do not allow the formation of catalytically active Brønsted acid sites [4]. Maximum activity is found at a specific surface density due to the formation of larger WO_x domains, which reduce more easily and allow the stabilization of a larger number of strong acidic sites by electron delocalization. At coverages above the monolayer, three-dimensional WO_3 crystallites start to develop on the zirconia surface, leading to decreased accessibility to the strong Brønsted acid sites. In the anion exchange preparation method at tungsten coverages below the monolayer, it was found from the Raman analysis that WO_x species have stronger interactions with the support; then, these W sites have more acid strength (TA, Fig. 2b). Above monotungstate coverage (7 W/nm^2 for ODS reactions [6]), the activity remains high, which is in contrast with the impregnation method (TA-700, Tables 1 and 3). This result can be ascribed to the fact that strong interactions of the WO_x species with the support are preserved when calcined at 700 °C (TA-700, Fig. 2b); in addition, a broad distribution of polytungstates appeared on the surface, which enhanced the Brønsted acidity, because larger WO_x domains create stronger acid sites. Another

issue is that WO_3 crystallites are absent, allowing free access of reactants to acid sites.

The preparation method is also important, impregnation is an accepted method because of its simplicity. Catalysts prepared by the coprecipitation method were found to contain twice the amount of strong acid sites and displayed higher activity for n-pentane isomerization, which is due to higher dispersion of the WO_x species on the zirconia surface. This fact retards the formation of WO_3 crystallites and allows the production of highly interconnected amorphous WO_x domains that are needed for the generation of catalytically active Brønsted acid sites [62]. On the other hand, the hydrothermal method yields stronger zirconium–tungsten interactions with strong Lewis acid sites, which remain even at 400 °C without the formation of the crystalline WO_x phase [41]. The two-phase interface hydrolysis method yields smaller average crystallite sizes and larger BET surface area in comparison with the impregnation method, where the formation of WO_3 crystallites is suppressed [63]. The acidity of the WO_x/ZrO_2 systems prepared by the impregnation method has been calculated by different methods; for example, ^{15}N CP MAS NMR of pyridine detected 0.03 mmol/g of Brønsted acid sites, and 0.09 mmol/g of Lewis acid sites [64]; on the other hand, a maximum total acidity of 0.107 mmol/g was found with NH$_3$-TPD with a W loading of 25 wt.% WO$_3$ [61]; as for the two-phase interface hydrolysis method, it produces a remarkable number of strong acid sites: 0.098 and 0.127 mmol/g of Brønsted and Lewis sites, respectively [63]. The exceptional acidity developed by the anion

Table 4
Removal of sulfur compounds in diesel fuel.

Compound	Removal (%)	Electron density [60]
4,6-dimethyldibenzothiophene	100	5.760
4-methyl dibenzothiopphene	100	5.759
Dibenzothiophene	100	5.758
Benzothiophene	52	5.739
Thiophene	20	5.696

exchange method (2.202 mmol/g), the presence of strong Brønsted and Lewis sites, which remain at 400 °C, and the presence of different acid strengths is in good agreement with the characteristics of these solids, which can be associated with: 1) better dispersion of the tungsten species, 2) low coordination of the W species, which are strongly anchored to the support, 3) the presence of a broad distribution of polytungstate species and 4) the absence or high dispersion of WO_3 crystallites.

3.6. Oxidative desulfurization of diesel fuel and SRGO

The TA-700 catalyst was tested in the desulfurization reaction using diesel fuel with γ-butyrolactone and methanol as solvents. The analysis for determining the sulfur families was made by gas chromatography; specific compounds were determined (Table 4). After the ODS reaction, methyldibenzothiophenes and C_1-C_3-dibenzothiophenes (the most refractory compounds in the hydrodesulfurization process, HDS) were fully removed in 30 min of reaction; the removal of the identified compounds followed the relationship of the electron density reported by Otsuky et al. [60]. The hydrocarbon phase was subjected to a washing step with fresh solvent; this step extracts residual sulfones dissolved in the hydrocarbon (Tables 5). The same reaction and washing step were carried out with non-hydrotreated SRGO; high levels of total sulfur removal were obtained (Table 6).

The total sulfur removal of the three different hydrocarbons used in this work is summarized in Fig. 10. We can observe that high levels of sulfur removal are obtained in short times. The apparent slowness of diesel fuel and SRGO after 15 min of reaction may be due to the decomposition of hydrogen peroxide into O_2 and water. This decomposition was reported in a previous study by measuring the amount of oxygen evolved during the reaction [29]; we found high decomposition levels of hydrogen peroxide in the ODS according to the following reaction:

$$H_2O_2 \rightarrow H_2O + O_2$$
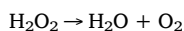
The high TOF obtained for SRGO is interesting (Table 3), because the initial curve is similar to that of diesel fuel, but the moles of reacted sulfur are much higher. In addition, this fuel has a high concentration of refractory compounds such as benzothiophenes and methylbenzothiophenes, which are easily removed.

Table 5
Desulfurization of diesel fuel.

	Butyrolactone as solvent		Methanol as solvent	
	S concentration (ppmw)	Desulfurization (%)	S concentration (ppmw)	Desulfurization (%)
I	338	–	338	–
II	82	75.7	118	65.1
III	10	97.0	79	76.6

I. Initial charge.
II. After the ODS reaction.
III. After the washing step.

Table 6
Desulfurization of SRGO.

	Butyrolactone as solvent		Methanol as solvent	
	S concentration (ppmw)	Desulfurization (%)	S concentration (ppmw)	Desulfurization (%)
I	16,370	–	16,370	–
II	5,828	64.4	6,379	61.0
III	4,957	69.7	5,846	62.3

I. Initial charge.
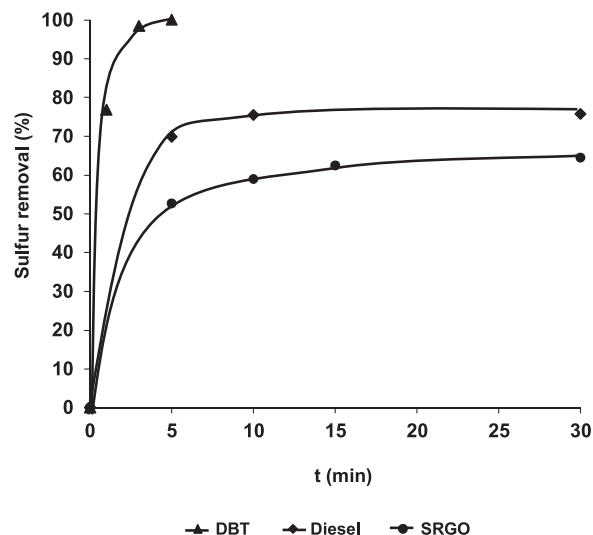II. After the ODS reaction.
III. After the washing step.

Fig. 10. Sulfur removal of DBT and sulfur compounds from diesel fuel and SRGO.

3.7. Denitrogenation of diesel fuel and SRGO

Denitrogenation of diesel fuel (45 ppm of total nitrogen) and SRGO (318 ppm of total nitrogen) was evaluated from the analytical analysis of the same reactions cited in 3.2 using the TA-700 catalyst. As seen in Table 7, denitrogenation attained high levels and the removal of these nitrogen compounds was achieved, as in the case of sulfur compounds, by the solvent. Other denitrogenation studies by oxidation have been published, for example, Shiraishi et al. performed the denitrogenation of SRGO and LCO with acetic acid and H_2O_2 in a two-step process (oxidation–extraction), obtaining 84% of reduction of nitrogen compounds in 30 h of reaction [23]. Ishihara et al. oxidized a pre-desulfurized LGO with a Mo/Al_2O_3 catalyst and *tert*-butyl hydroperoxide in a two-step process (denitrogenation-extraction), decreasing the N-compounds from an initial value of 13.5 ppm to a final value of 0.8 ppm [24].

The deep removal of nitrogen compounds, here reported, in short reaction times is attributed to the elevated activity of the WO_x/ZrO_2 catalyst in a similar way to the desulfurization process. Further studies regarding the influence of the nature of the nitrogen compounds as well as the oxidation products formed in these reactions will be reported in a future paper.

In order to test these catalysts in severe environments, the SRGO was subjected to a treatment to obtain a concentrated hydrocarbon with higher nitrogen concentration. This was performed using a selective nitrogen-adsorption material in the following way: the selective nitrogen-adsorption material was packed in a column and the SRGO was pumped at a constant up flow. Samples were taken at different times and analyzed until the nitrogen concentration of the output flow

Table 7
Denitrogenation of diesel and SRGO using butyrolactone as solvent.

	Diesel fuel		SRGO	
	N concentration (ppmw)	Denitrogenation (%)	N concentration (ppmw)	Denitrogenation (%)
I	45	–	318	–
II	4	91.8	42	86.8
III	2	95.6	35	89.0

I. Initial charge.
II. After the ODS reaction.
III. After the washing step.

Table 8
Denitrogenation of a concentrated hydrocarbon.

	Butyrolactone as solvent		Methanol as solvent	
	N concentration (ppmw)	Denitrogenation (%)	N concentration (ppmw)	Denitrogenation (%)
I	4,161	–	4,161	–
II	704	83.1	2,092	49.7
III	347	91.7	2,050	50.7
IV	213	95.0	1,031	75.2

I. Initial charge.
II. After the ODS reaction.
III. After the first washing step.
IV. After the second washing step.

Table 9
Desulfurization of a concentrated hydrocarbon.

	Butyrolactone as solvent		Methanol as solvent	
	S concentration (ppmw)	Desulfurization (%)	S concentration (ppmw)	Desulfurization (%)
I	28,571	–	28,571	–
II	4,794	83.2	8,497	70.3
III	3,948	86.2	7,960	72.0
IV	3,154	89.0	7,407	74.1

I. Initial charge.
II. After the ODS reaction.
III. After the first washing step.
IV. After the second washing step.

equaled the concentration of the input flow. Once the adsorbent has been exhausted, the column was drained, and an acetone flow was passed until this came out without staining, which indicated that the adsorbent had been cleaned from the adsorbed compounds. The acetone mixture with the concentrated hydrocarbon was distilled, recovering acetone after condensation. The concentrated hydrocarbon had 4161 ppm of total nitrogen.

This concentrated sample was subjected to an oxidation treatment followed by two washing steps with fresh solvents. The reaction time was set to 1 h, maintaining the other conditions used for diesel fuel and SRGO. The results are shown in Table 8. The initial concentrated hydrocarbon had a dark color while the final product had a light amber color. High denitrogenation levels were obtained up to 95%. These results proved the elevated removal of contaminants obtained with tungstated-zirconia catalysts synthesized by ionic exchange from tungstic acid as precursor. From the results of the present work, tungsten/zirconia catalysts removed efficiently nitrogen compounds; to date, this system has not been reported for nitrogen removal.

Although the material used to concentrate the SRGO was nitrogen-selective, sulfur compounds were also concentrated, giving a final value of 28,571 ppm of these compounds; the desulfurization level reached in the same reaction was 89% (Table 9).

The ODS process has many challenges in order to be used as a stand-alone approach, and one of them is to develop more active catalysts. It has been proposed to be used as a post-treatment of the hydro-desulfurization process, which in order to remove refractory molecules such as 2,4-dimethyl dibenzothiophene, the reaction conditions must be more severe. As the ODS makes these refractory molecules react easily, ultra-clean fuels can be obtained by combining both processes.

The results show that other heavy fractions such as SRGO from cocker plants or light cyclic oil can be treated with oxidative de-sulfurization; these streams can contain from 20,000 to 25,000 ppm of total sulfur or even more if they are obtained from heavy crude oil. ODS can be used to pretreat heavy hydrocarbons with high sulfur content and remove around 70 and 90% of these sulfured and nitrogenated compounds, respectively. The stream from this approach can then be treated in a conventional HDS system, which will treat a stream with lower sulfur loads, less hydrogen consumption and probably with milder operating conditions. Nevertheless, other items must be considered such as the investment, operating costs and engineering issues.

4. Conclusions

The preparation method of tungsten/zirconia catalysts is very important to obtain efficient catalysts for ODS reactions. Anionic exchange at low pH, using peroxotungstic acid is reported. The main characteristics of the anion exchange method that are different from those obtained with ammonium metatungstate are: tetrahedral species are generated even at high W contents without the formation of WO_3 crystallites; it creates one order of magnitude more acidity than the impregnation method; strong and weak Brønsted and Lewis sites with improved homogeneity of the WO_x species are present in these catalysts. The nature of the acid sites in both catalysts is different, generating their acidity by different tungsten oxidation states.

Oxidative denitrogenation and oxidative desulfurization of DBT, diesel fuel, SRGO and a concentrated hydrocarbon were achieved at high levels and short times as a one-process applied to obtain clean fuels; further washing steps assured the removal of residual sulfones and oxidized nitrogen compounds.

From theoretical results, it is shown that peroxide reacts more

favorably with octahedral-coordination catalysts than with those displaying a tetrahedral one. However, the analysis of molecular orbitals reveals that the tetrahedral coordination on the activated catalyst favors more the oxidative desulfurization of DBT than the octahedral one, due to the fact that the electron transfer during the DBT conversion occurs from DBT to the catalyst, enabling the catalyst to be continuously available to react with peroxide whereas the octahedral coordination promotes the electron transfer from the catalyst to DBT, which is a step that releases less energy.

Acknowledgment

References

[1] M.R. Khan, E. Al-Sayed, Energy Sources Part A 30 (2008) 200–217.
[2] Z. Ismagilov, S. Yashnik, M. Kerzhentsev, V. Parmon, A. Bourane, F.M. Al-Shahrani, A.A. Hajji, O.R. Koseoglu, Catal. Rev. Sci. Eng. 53 (2011) 199–255.
[3] S. Kuba, P. Lukinskas, R.K. Grasselli, B.C. Gates, H. Knözinger, J. Catal. 216 (2003) 353–361.
[4] A. Martínez, G. Prieto, M.A. Arribas, P. Concepción, J.F. Sánchez-Royo, J. Catal. 248 (2007) 288–302.
[5] M. Valigi, D. Gazzoli, I. Pettiti, G. Mattei, S. Colonna, S. De Rossi, G. Ferraris, Appl. Catal. A 231 (2002) 159–172.
[6] G. Rodriguez-Gattorno, A. Galano, E. Torres-García, Appl. Catal. B 92 (2009) 1–8.
[7] Z. Hasan, J. Jeon, S.H. Jhung, J. Hazard. Mater. 205–206 (2012) 216–221.
[8] L.F. Ramírez-Verduzco, J.A. de los Reyes, E. Torres-García, Ind. Eng. Chem. Res. 47 (2008) 5353–5361.
[9] F. Figueras, J. Palomeque, S. Loridant, C. Fèche, N. Essayem, G. Gelbard, J. Catal. 226 (2004) 25–31.
[10] F. Figueras, N. Essayem, C. Fèche, S. Loridant, J. Palomeque, G. Gelbard, US Pat. 7851401 B2, 2010.
[11] M.J. Girgis, B.C. Gates, Ind. Eng. Chem. Res. 30 (1991) 2021–2058.
[12] S.A. Hanafi, M.S. Mohamed, Energy Sources Part A 33 (2011) 495–511.
[13] M.Y. Lui, L. Cattelan, L.C. Player, A.F. Masters, A. Perosa, M. Selva, T. Maschmeyer, Energy Fuels 31 (3) (2017) 2183–2189.
[14] I. Ahmed, S.H. Jhung, J. Hazard. Mater. 301 (2016) 259–276.
[15] J.-M. Kwon, J.-H. Moon, Y.-S. Bae, D.-G. Lee, H.-C. Sohn, C.-H. Lee, ChemSusChem 1 (2008) 307–309.
[16] L.-L. Xie, A. Favre-Reguillon, X.-X. Wang, X. Fu, M. Lemaire, J. Chem. Eng. Data 55 (2010) 4849–4853.
[17] I. Ahmed, S.H. Jhung, Chem. Eng. J. 279 (2015) 327–334.
[18] S.K. Thaligari, S. Gupta, V.C. Srivastava, B. Prasad, Energy Fuels 30 (2016) 6161–6168.
[19] J.H. Kim, X. Ma, A. Zhou, C. Song, Catal. Today 111 (2006) 74–83.
[20] N.A. Khan, S.H. Jhung, Inorg. Chem. 54 (23) (2015) 11498–11504.
[21] P. Forte, A. Sachse, M. Maes, A. Galarneau, D. de Vos, RSC Adv. 4 (3) (2014) 1045–1054.
[22] S. Zhang, Q. Zhang, Z.C. Zhang, Ind. Eng. Chem. Res. 43 (2004) 614–622.
[23] Y. Shiraishi, K. Tachibana, T. Hirai, I. Komasawa, Ind. Eng. Chem. Res. 41 (2002) 4362–4375.
[24] A. Ishihara, D. Wang, F. Dumeignil, H. Amano, E.W. Qian, T. Kabe, Appl. Catal. A 279 (2005) 279–287.
[25] E. Rafiee, S. Rezaei, J. Taiwan Inst. Chem. Eng. 61 (2016) 174–180.
[26] T. Kim, A. Burrows, C.J. Kiely, I.E. Wachs, J. Catal. 246 (2007) 370–381.
[27] J. Macht, C.D. Baertsch, M. May-Lozano, S.L. Soled, Y. Wang, E. Iglesia, J. Catal. 227 (2004) 479–491.
[28] C.D. Baertsch, S.L. Soled, E. Iglesia, J. Phys. Chem. B 105 (2001) 1320–1330.
[29] J. Palomeque, J.M. Clacens, F. Figueras, J. Catal. 211 (2002) 103–108.
[30] L.F. Ramírez-Verduzco, E. Torres-García, R. Gomez-Quintana, V. Gonzalez-Peña, F. Murrieta-Guevara, Catal. Today 98 (2004) 289–294.
[31] D.G. Barton, S.L. Soled, G.D. Meitzner, G.A. Fuentes, E. Iglesia, J. Catal. 181 (1999) 57–72.
[32] D.G. Barton, M. Shtein, R.D. Wilson, S.L. Soled, E. Iglesia, J. Phys. Chem. B (103) (1999) 630–640.
[33] E. Briot, J.-Y. Piquemal, M. Vennat, J.-M. Brégeault, G. Chottard, J.-M. Manoli, J. Mater. Chem. 10 (2000) 953–958.
[34] S. Ji, T. Xiao, S. Li, L. Chou, B. Zhang, C. Xu, R. Hou, A.P.E. York, M.L.H. Green, J. Catal. 220 (2003) 47–56.
[35] M. Scheithauer, R.K. Grasselli, H. Knözinger, Langmuir 14 (1998) 3019–3029.
[36] T.R. Ravindran, A.K. Arora, T.A. Mary, J. Phys. Condens. Matter 13 (2001) 11573–11588.
[37] J.R. Sohn, M.Y. Park, Langmuir 14 (1998) 6140–6145.
[38] P. Wongmaneenil, B. Jongsomjit, P. Praserthdam, Catal. Commun. 10 (2009) 1079–1084.
[39] S.R. Vaudagna, R.A. Comelli, N.S. Fígoli, Appl. Catal. A 164 (1997) 265–280.
[40] E. Torres-García, G. Rosas, J.A. Ascencio, E. Haro-Poniatowski, R. Pérez, Appl. Phys. A 79 (2004) 401–406.
[41] H. Armendáriz, M.A. Cortes, I. Hernández, J. Navarrete, A. Vázquez, J. Mater. Chem. 13 (2003) 143–149.
[42] R.G. Rodríguez Avendaño, J.A. De Los Reyes, T. Viveros, J.A. Montoya de la Fuente, Catal. Today 148 (2009) 12–18.
[43] A. Bazyari, A.A. Khodadadi, A.H. Mamaghani, J. Beheshtian, L.T. Thompson, Y. Mortazavi, Appl. Catal. B 180 (2016) 65–77.
[44] B. Zhang, Z. Jiang, J. Li, Y. Zhang, F. Lin, Y. Liu, C. Li, J. Catal. 287 (2012) 5–12.
[45] K.Y.S. Ng, E. Gulari, Polyhedron 3 (8) (1984) 1001–1011.
[46] D. Gazzoli, M. Valigi, R. Dragone, J. Phys. Chem. B 101 (1997) 11129–11135.
[47] S. Loridant, C. Feche, N. Essayem, F. Figueras, J. Phys. Chem. B 109 (2005) 5631–5637.
[48] S. Naito, N. Katada, M. Niwa, J. Phys. Chem. B 103 (1999) 7206–7213.
[49] F. Di Gregorio, V. Keller, J. Catal. 225 (2004) 45–55.
[50] J. Bernholc, J.A. Horsley, L.L. Murrell, L.G. Sherman, S. Soled, J. Phys. Chem. 91 (1987) 1526–1530.
[51] M.A. Cortés-Jácome, C. Angeles-Chavez, E. López-Salinas, J. Navarrete, P. Toribio, J.A. Toledo, Appl. Catal. A 318 (2007) 178–189.
[52] A. Galano, G. Rodriguez-Gattorno, E. Torres-García, Phys. Chem. Chem. Phys. 10 (2008) 4181–4188.
[53] I.W.C.E. Arends, R.A. Sheldon, Appl. Catal. A 212 (2001) 175–187.
[54] V. Hulea, A.-L. Maciuca, F. Fajula, E. Dumitriu, Appl. Catal. A 313 (2006) 200–207.
[55] D. Wang, E.W. Qian, H. Amano, K. Okata, A. Ishihara, T. Kabe, Appl. Catal. A 253 (2003) 91–99.
[56] Z.E.A. Abdalla, B. Li, A. Tufail, J. Ind. Eng. Chem. 15 (2009) 780–783.
[57] J.L. García-Gutiérrez, G.A. Fuentes, M.E. Hernández-Terán, F. Murrieta, J. Navarrete, F. Jiménez-Cruz, Appl. Catal. A 305 (2006) 15–20.
[58] J. Arichi, M. Eternot, B. Louis, Catal. Today 138 (2008) 117–122.
[59] W.N.A.W. Mokhtar, W.A.W.A. Bakar, R. Ali, A.A.A. Kadir, Clean Technol. Environ. Policy 17 (2015) 1487–1497.
[60] S. Otsuki, T. Nonaka, N. Takashima, W. Qian, A. Ishihara, T. Imai, T. Kabe, Energy Fuels 14 (2000) 1232–1239.
[61] W. Ciptonugroho, M.G. Al-Shaal, J.B. Mensah, R. Palkovits, J. Catal. 340 (2016) 17–29.
[62] D.C. Calabro, J.C. Vartuli, J.G. Santiesteban, Top. Catal. 18 (2002) 231–242.
[63] K. Song, H. Zhang, Y. Zhang, Y. Tang, K. Tang, J. Catal. 299 (2013) 119–128.
[64] K. Shimizu, T.N. Venkatraman, W. Song, Appl. Catal. A 224 (2002) 77–87.